Jpn. J. Appl. Phys. Vol. 38 (1999) pp. L 174–L 177
Part 2, No. 2B, 15 February 1999

Ion Energy Distribution in Alternating-Current Plasma Display Panel Cell

Young Kyo SHIN, Jae Koo LEE*, Chae Hwa SHON and Woong KIM
Department of Physics, Pohang University of Science and Technology, Pohang 790-784, S. Korea

(Received October 13, 1998; accepted for publication December 28, 1998)

In an alternating-current plasma display panel cell, elastic collisions between the neutral gas and ions keep most ion energies much lower than the applied voltage. Two-dimensional kinetic simulation reveals that the majority (90%) of the plasma ions impinging on the dielectric layer have energy at or below 10% of the applied voltage of 250 V calling for the need for measurement of the secondary electron emission-coefficient below 50 eV. The kinetic potential and density profiles compare well with those of a two-dimensional fluid simulation.

KEYWORDS: plasma display, simulation, energy distribution, kinetics, secondary emission

Plasma display panel (PDP) is one of the most promising candidates for high definition color television (HDTV).[1] Because fluid simulations[2–5] employ only the quantities averaged over the velocity distribution, they have limitations when it comes to examine the kinetic phenomena inside the cell. Kinetic phenomena occur in the sheath whose size is comparable with the cell size. Kinetic simulations have a unique capability of calculating the energy distributions, which are important in order to understand the characteristics of the PDP cell. The ion energy distribution is an important factor during determination of the ion current density, which is obtained by integrating the distribution function over the velocity space and affects the erosion rate of the dielectric layer and the secondary electron emission-coefficient γ_{se}. The elastic mean-free path of an ion is in the sub-micrometer range in a typical PDP cell. Ions undergo many collisions with neutral gases as they are accelerated by the electric potential difference toward the dielectric layer. The energy of ions impinging on the dielectric layer is calculated to be much lower than the applied voltage.

The cell geometry is shown in Fig. 1(a), where the cell size is 1260×210 μm^2. The neutral gas is neon with the gas pressure of 500 Torr and an external voltage of 250 V is applied to the V_x electrode. V_y and V_a electrodes are grounded. Dielectric layers of 30 μm thickness are deposited above the electrodes, the dielectric constant is 10. MgO serves as the protective layer and the source of the secondary electrons emitted with γ_{se}. We consider the MgO effect with γ_{se} of the dielectric layer, which is assumed to be $\gamma_{se} = 0.5$ for neon. In our simulation, we use a particle-in-cell/Monte Carlo (PIC/MC) two-dimensional simulation code, OOPIC.[6] OOPIC code uses the Monte Carlo collisions with three velocity components, v_x, v_y, and v_z, to obtain the collision rates. The simulated particles which correspond to the density of 1.89×10^{15} m^{-3} have velocities and positions that are calculated self consistently. Figure 1(b) shows the number of ions and electrons as a function of time. A difference in density between ions and electrons occurs near the cathode shown in Figs. 3(b) and 3(c).

Electron and ion energy distributions are important for many practical purposes. We calculate the distribution of the y-component of the particle velocity in a given region at a specified y-location. Figures 2(a)–2(d) show the ion energy distribution function (IEDF) at two different positions, in front of the dielectric layer at the cathode side and in the bulk plasma, at two different times. Each particle has a velocity and a position at any given time. We obtain a phase space plot, the velocity distribution along the y direction, from which the energy distribution is obtained by arranging and squaring the velocities in a given region Δy. Ion energy distributions are plotted in a semi-log scale with the energy indicated in the abscissa which is divided into 150–200 cells. The number of particles at the corresponding energy region is shown in the ordinate. The total area below the points is the total number of particles existing in a given region. The IEDFs of the bulk plasma are shown in Figs. 2(a) and 2(b). Figure 2(a) is the IEDF at the initial stage of ionization at $t = 22$ ns. 90% of the ions located between 100 μm and 180 μm have energy below 1 eV. The bulk plasma is nearly field free with the accomplishment of charge neutrality. The distribution is Maxwellian other than at the cathode sheath. The charge accumulation in the dielectric layer results in a drop of the applied voltage during migration of the ions to the cathode. The region of the flat potential moves to the cathode in a fashion similar to the ionization wave shown in Fig. 3(a). The IEDF between 55 μm and 180 μm at $t = 37$ ns is shown in Fig. 2(b). The result is similar to that of Fig. 2(a).

The results of Figs. 2(c) and 2(d) show that the ion energy distributions have two slopes. Figure 2(d) shows the IEDF when the number density is maximum at 37 ns. Generally, the sheath voltage is nearly equal to the gap voltage, thus ions can be accelerated to the gap voltage. The majority of ion energy in the simulation is below 50 eV. The reasons for low ion energy are as follows. First, high neutral gas of 300–600 Torr causes many elastic collisions with the ions. The elastic mean-free path is $\lambda_{el} = 1/n_g\sigma_{el}$, with neutral gas density, $n_g = 3.26 \times 10^{16} p$ Torr·cm^{-3}, and elastic cross sec-

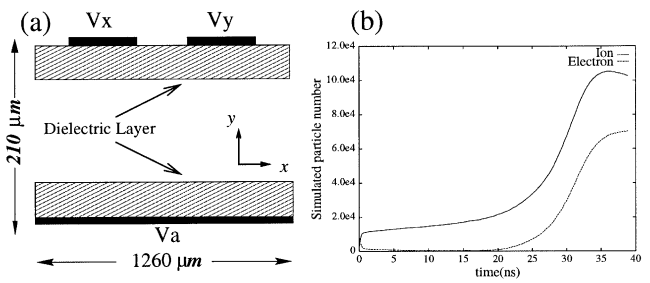

Fig. 1. (a) Cell geometry, 1260×210 μm^2, $V_x = 250$ V, $V_y = V_a = 0$ V, dielectric constant $\epsilon_r = 10$. (b) Kinetic simulation of number of ions (solid) and electrons (dashed), each particle represents the density 1.890×10^{15}m^{-3}.

*E-mail address: jkl@postech.ac.kr

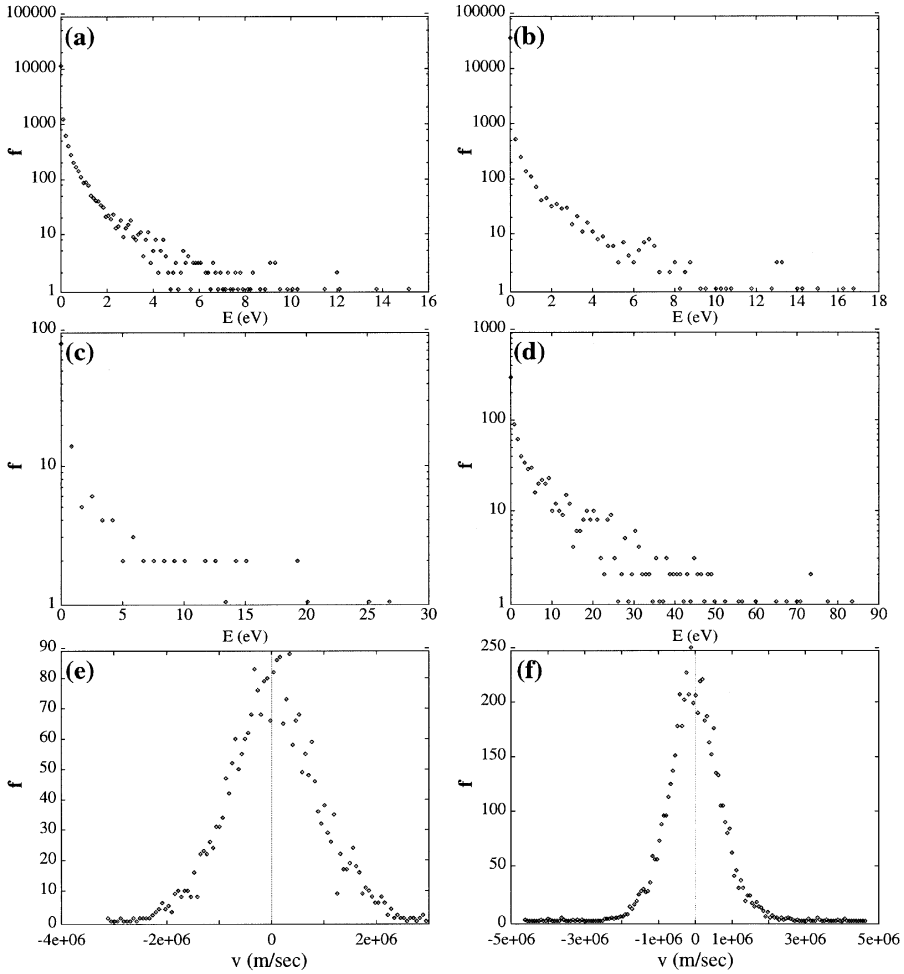

Fig. 2. Kinetic energy distributions: (a) and (b) for the ion energy distribution in the bulk plasma at 22 ns (100–180 μm) and 37 ns (55–180 μm), (c) and (d) for the ion energy distribution of the cathode sheath at 22 ns (30–35 μm) and 37 ns (30–35 μm), (e) and (f) for the electron velocity distribution in bulk plasma at 22 ns and in the cathode sheath at 37 ns.

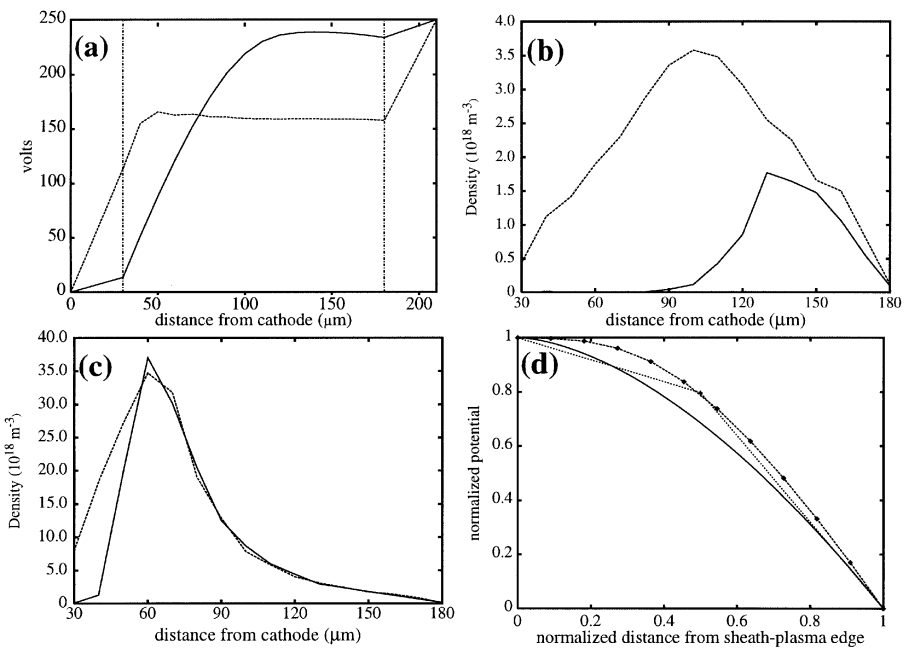

Fig. 3. Kinetic simulations, the cross section along the y-direction at the center of V_x electrode: (a) potential profile at 22 ns (solid), 37 ns (dotted) dielectric layer (solid and dotted), (b) and (c) electron (solid) and ion (dotted) density cross section at the center of the electrode at 22 ns and 37 ns, (d) the normalized potential profile, comparison of the results obtained from theory (solid) with those from the simulation (dots for 22 ns and dotted line for 37 ns).

tion $\sigma_{el} = 5\text{–}20 \times 10^{-16}$ cm^2 for neon.[7] From these data, the elastic mean-free path of an ion is in the range of 0.3–1.2 μm. Ions are highly collisional inside the sheath because the sheath size is 10–50 μm. Although a high electric field is applied in the sheath region, ions do not obtain sufficient energy from the electric field because of the frequent elastic collisions with the neutral gas. In a magnetron discharge, a gas pressure of 5–20 mTorr is required to make the system collisionless. The ions in the cathode region are accelerated to 300–350 volts, which is 80–90% of the applied voltage.[8] Another reason for the low ion energies is the potential drop across the cell. Figure 3(a) shows that the potential difference at 37 ns between 30 and 50 μm is less than 50 eV, which is the energy to accelerate an ion from the bulk (flat potential region) to the dielectric layer at 30 μm. This is because of the charge accumulations on both sides of the dielectric surfaces. Most experiments measuring γ_{se} are performed above 50 eV[9] while the energy of ions impinging on the dielectric is below 50 eV. For neon, when the energies of incident ions at the MgO are 50, 100, and 150 eV, γ' s are 0.08, 0.11, and 0.13, respectively according to the published data in ref. 10. γ plays an important role in discharge initiation and self-sustainment. An accurate measured value for γ in the low-energy range below 50 eV is needed for many purposes including simulations.

We obtain the space and time dependent distribution function for electrons as well as for ions; this is different from the fluid model using the assumed distribution. The kinetic distribution of electrons generates more accurate collision rates. Figures 2(e) and 2(f) are the electron velocity distributions in the bulk at 22 ns and the sheath regions at 37 ns, respectively. Electron velocity distributions are Maxwellian except for in the sheath region. Ion and electron density profiles are shown in Figs. 3(b) and 3(c). Charge neutrality is accomplished with a flat potential. It is not necessary to use the two-dimensional simulation; the qualitative nature is similar in the one-dimensional simulation which we also carried out. If we require the current density profile which plays an important role in the erosion rate at the cathode, we need to perform two-dimensional simulations. The plot along the y direction at the center of the V_x electrode shows the density profile, the degree of the charge neutrality, and the potential profile as a function of time. As the discharge proceeds, the charge neutrality is accomplished.

We verify the elastic collision effect in the sheath with the model of the collisional sheath whose ion current density J_i[7] is

$$J_i = \left(\frac{2}{3}\right)\left(\frac{5}{3}\right)^{3/2} \epsilon_0 \left(\frac{2e\lambda_i}{\pi M}\right)^{1/2} \frac{V_0^{3/2}}{s^{5/2}}. \quad (1)$$

Here, M, V_0, s, and ϵ_0 are ion mass, sheath voltage, sheath size, and permittivity of free space, respectively. J_i values are 49.3 mA/cm^2 and 142.4 mA/cm^2 taking $\lambda_i = 0.7\mu$m at 22 ns and 37 ns, respectively. Sheath potentials are 225 V and 52.3 V, sheath sizes are 110 μm and 30 μm at two different times, 22 ns and 37 ns, respectively. We obtain the potential profile in the sheath region integrating Poisson's equation assuming that the ionization within the sheath region is negligible and the current density is constant in the region. The potential profile in the sheath is

$$\frac{\phi}{V_0} = 1 - \left(\frac{x}{s}\right)^{\frac{5}{3}}, \quad (2)$$

where $x = 0$ is the plasma-sheath edge and $x = 1$ the dielectric layer. Figure 3(d) shows the normalized potential profile in the sheath region. Solid, dashed, and dotted lines indicate the theoretical curve given by eq. (2), at 22 ns and 37 ns, respectively. The potential is normalized with the voltage difference between the plasma-sheath edge and the dielectric layer. Simulation results coincide well with the theoretical curve. The high normalized potential results from the

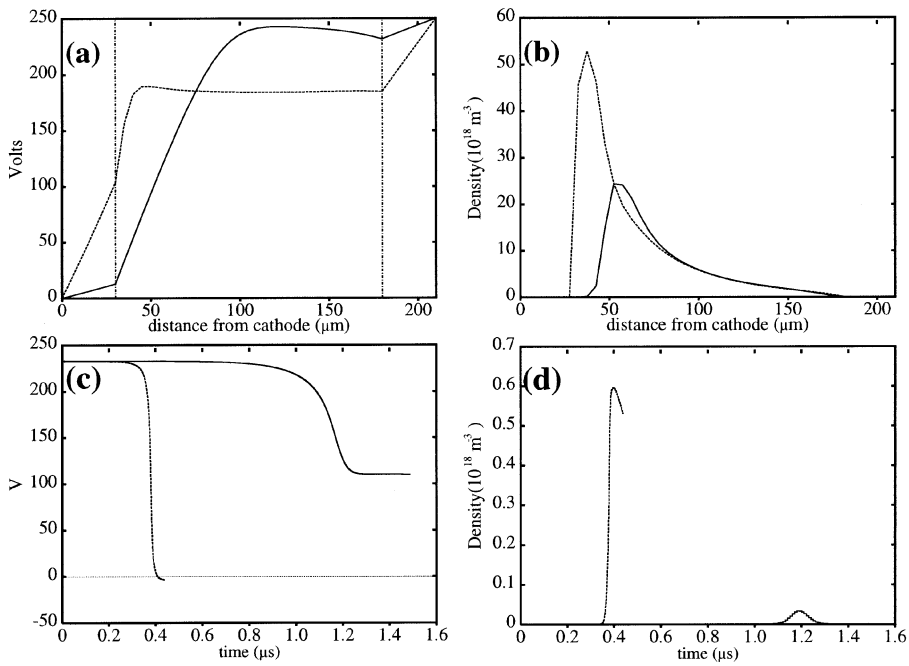

Fig. 4. Fluid simulation, the cross section along the y-direction at the center of V_x electrode: (a) potential, (b) electron and ion density, (c) potential difference between dielectric layers, (d) average electron density with γ_{Neon} = 0.5 (dotted) and 0.05 (solid).

ionization in the sheath, which is neglected in the theoretical model. The ionization avalanche occurs at 22 ns, when many ionization events exist, especially in front of the flat potential in $x = 0$–0.2. Electrons created by ionization leave the sheath region faster than ions because of their large mobilities and large elastic mean-free path which is on the order of 1.4–4.3 μm. Thus, the sheath region has many ions more than the theoretical model neglecting the ionization in the sheath. These ions results in the high potential.

We use the fluid simulation to show the effect of variation of γ_{se} due to the low energy of ions impinging on the dielectric layer. Figures 4(a) and 4(b) show the fluid simulation using the input parameters of the kinetic simulation except for Ne–Xe (90/10 %) mixed gas with the potential and the density profiles at different times, similar to those of the kinetic simulation. For the mixed gas, the low ionization energy of xenon gas increases the plasma densities. Since the majority (90%) of the plasma ions impinging on the dielectric layer have energy at or below 10% of the applied voltage of 250 V, another fluid simulation with γ_{Neon} set to 0.05 is performed for comparison and showing the important role of γ_{se} in the discharge. Figure 4(c) shows the voltage transferred to the dielectric layer for $\gamma_{Neon} = 0.5$ and 0.05. 60% of the applied voltage is transferred to the dielectric layer for $\gamma_{Neon} = 0.05$ while 100% of the applied voltage is transferred to the dielectric layer for $\gamma_{Neon} = 0.5$. After the discharge is extinguished, the remaining voltage in the case of $\gamma_{Neon} = 0.5$ breaks the charge neutrality. Figure 4(d) shows the average electron density with $\gamma_{Neon} = 0.5$ and 0.05, respectively. The average electron density is reduced to 5% of the $\gamma_{Neon} = 0.5$ result.

In summary, the ion energy-distributions near the dielectric layer were obtained using the kinetic code shown in Fig. 2. Short elastic mean-free path and charge accumulations on the dielectric layers caused very low ion energies at the dielectric layer near the cathode. Most of the ion energies in the cathode sheath were below 50 eV. This low energy affected γ_{se}. The fluid result of varying γ_{Neon} for neon showed the important role of γ in discharge initiation and wall voltage transfer. As there are no γ_{se} measurements on MgO available at present for the energy of impinging ions of below 50 eV, we showed the need for γ_{se} measurement in the future in the region of low ion energy. We compared the potential profile with the collisional Child's law to verify the collisional sheath. The details of the ion energy-distribution are also important in connection with sputtering and erosion of the layer.

This work was supported by the PDP Research Center, the BSRI-Special Fund of POSTECH, and the Basic Science Research Institute Program, Ministry of Education, Project No. 98-2439.

1) A. Sobel: IEEE Trans. Plasma Sci. **19** (1991) 1031.
2) C. Punset, J. P. Boeuf and L. C. Pitchford: J. Appl. Phys. **83** (1998) 1884.
3) R. Veerasingam, R. B. Campbell and R. T. McGrath: Plasma Sources Sci. Technol. **6** (1997) 157.
4) J. K. Lee, L. Meng, Y. K. Shin, H. J. Lee and T. H. Chung: Jpn. J. Appl. Phys. **36** (1997) 5714.
5) K. Takahashi, S. Hashiguchi, Y. Murakami, M. Takei, K. Itoh, K. Tachibana and T. Sakai: Jpn. J. Appl. Phys. **35** (1996) 251.
6) J. P. Verboncoeur, A. B. Langdon and N. T. Gladd: Comp. Phys. Commun. **87** (1995) 199.
7) M. A. Lieberman and A. J. Lichtenberg: *Principles of Plasma Discharges and Materials Processing* (John Wiley and Sons, Inc., New York, 1994).
8) C. H. Shon, J. K. Lee, H. J. Lee, Y. K. Shin, Y. Yang and T. H. Chung: to be published in IEEE Trans. Plasma Sci. **26** (1998) No. 6.
9) K. S. Moon: *Proc. 18th Int. Display Research Conf., Seoul 1998,* p. 403.